Effect of DNA Hairpin Loops on the Twist of Planar DNA Origami Tiles

ARTICLE *in* LANGMUIR · NOVEMBER 2011

Impact Factor: 4.46 · DOI: 10.1021/la2037873 · Source: PubMed

4 AUTHORS, INCLUDING:

Zhe li
Arizona State University
11 PUBLICATIONS **260** CITATIONS
SEE PROFILE

Hao Yan
National Cheng Kung University
28 PUBLICATIONS **942** CITATIONS
SEE PROFILE

Yan Liu
Arizona State University
151 PUBLICATIONS **6,833** CITATIONS
SEE PROFILE

Published in final edited form as:
Langmuir. 2012 January 31; 28(4): 1959–1965. doi:10.1021/la2037873.

Effect of DNA Hairpin Loops on the Twist of Planar DNA Origami Tiles

Zhe Li[†], **Lei Wang**[†,‡], **Hao Yan**[†], and **Yan Liu**[*,†]

[†]Department of Chemistry and Biochemistry, and the Biodesign Institute, Arizona State University, Tempe, Arizona 85287, United States

[‡]School of Pharmaceutical Sciences, Shandong University, Jinan 250012, P. R. China

Abstract

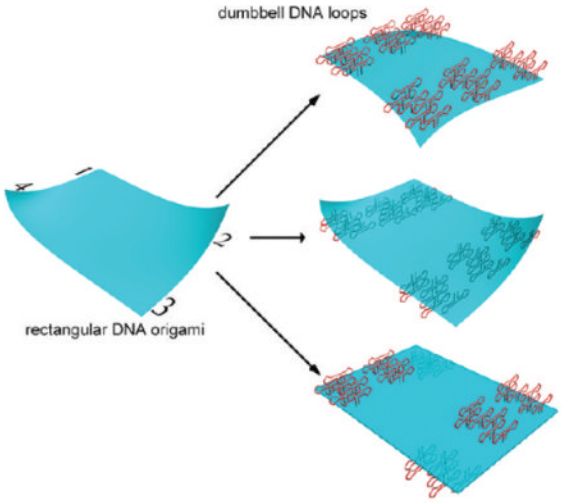

The development of scaffolded DNA origami, a technique in which a long single-stranded viral genome is folded into arbitrary shapes by hundreds of short synthetic oligonucleotides, represents an important milestone in DNA nanotechnology. Recent findings have revealed that two-dimensional (2D)DNA origami structures based on the original design parameters adopt a global twist with respect to the tile plane, which may be because the conformation of the constituent DNA (10.67 bp/turn) deviates from the natural B-type helical twist (10.4 bp/turn). Here we aim to characterize the effects of DNA hairpin loops on the overall curvature of the tile and explore their ability to control, and ultimately eliminate any unwanted curvature. A series of dumbbell-shaped DNA loops were selectively displayed on the surface of DNA origami tiles with the expectation that repulsive interactions among the neighboring dumbbell loops and between the loops and the DNA origami tile would influence the structural features of the underlying tiles. A systematic, atomic force microscopy (AFM) study of how the number and position of the DNA loops influenced the global twist of the structure was performed, and several structural models to explain the results were proposed. The observations unambiguously revealed that the first generation of rectangular shaped origami tiles adopt a conformation in which the upper right (corner 2) and bottom left (corner 4) corners bend upward out of the plane, causing linear superstructures

[*]Corresponding Author: yan_liu@asu.edu.

Supporting Information. DNA sequences, materials and additional AFM results. This material is available free of charge *via* the Internet at http://pubs.acs.org.

attached by these corners to form twisted ribbons. Our experimental observations are consistent with the twist model predicted by the DNA mechanical property simulation software CanDo. Through the systematic design and organization of various numbers of dumbbell loops on both surfaces of the tile, a nearly planar rectangular origami tile was achieved.

INTRODUCTION

Over the past two decades, DNA molecules have been rationally designed to self-assemble into various one-, two-, and three-dimensional (1D, 2D, and 3D) DNA nanostructures through sequence specific hybridization.[1–26] A large variety of chemical and biological components have been precisely organized into functional nanomaterials by these nanostructures.[27–38] Recently, various scaffolded DNA origami strategies have been developed to create complex and fully addressable patterns that have been widely utilized to design 2D and 3D[39–48] structures for the organization of functional molecules including proteins, nano-particles, and carbon nanotubes, and to perform single molecule chemical reactions with spatial control.[31,49–57]

The self-assembly of homogeneous or heterogeneous structural units into higher-order periodic or aperiodic architectures is one of the major challenges in nanotechnology. Similar to small branched DNA motifs, individual DNA origami tiles with the proper sticky end design will also self-assemble into larger super-structures with more complex structural features.[39,58,59] A simple example of this is the assembly of elongated nanoribbons.[60,61]

In a recent study we observed that planar, rectangular-shaped DNA origami tiles (based on original design specifications) formed both straight and twisted nanoribbon superstructures when assembled by complementary sticky end association.[60] The hierarchical assembly strategy of the tiles is illustrated in Figure 1. First, the cores of the origami tiles are assembled, excluding the extreme left and right columns of staples. Each of the four corners of the tiles are specified as 1, 2, 3, and 4, and contain 6 sections (16 nt each) of unpaired M13 scaffold strand. Linker strands are designed with two binding domains, one complementary to the unpaired region of M13 in one corner (e.g., corner 1), and the other complementary to the unpaired region of M13 in the opposite, diagonal corner (e.g., corner 3). Thus, 12 1′–3′ linker strands are used to arrange the preassembled origami cores into a stair-like ribbon structure (1–3 direction). Similarly, 12 2′–4′ linker strands connect the origami cores in the 2–4 direction.

1D stair-like ribbons with a maximum length of ~40 tiles were observed when linked by corners 1 and 3, while right-handed helical superstructures, with a half twist every other tile, were the product of linking corners 2 and 4. These observations suggested a significant twisting within the tile, very obvious in the 2–4 direction but negligible in the 1–3 direction. The conclusion was that the global twist deformation in the origami unit tile prevented extended growth of nanoribbons in the 2–4 direction.[60]

Single stranded DNA loops that adopt a dumbbell shaped structure are commonly utilized as topographic markers in DNA self-assembly.[49] However, attaching such a structure to the surface of a DNA tile can influence the features of the underlying tile because of the repulsive interactions among neighboring loops and between the loops and the tile. The magnitude of the repulsion likely depends on the interloop distance and relative position on the DNA tile. In this report we show that the undesired structural curvature of a rectangular shaped DNA origami tile can be rationally manipulated by attaching a series of dumbbell-shaped DNA loops at selected positions on the surface of the tiles. A systematic study was performed to determine how the number and position of the loops affect the degree of global

twisting of the underlying tile. Several arrangements of loops were successfully used to diminish the undesired curvature of a rectangular origami tile.

RESULTS AND DISCUSSION

The top and bottom surfaces of rectangular shaped DNA origami tiles are distinct from each other. Moving clockwise, the surface in which corners 1–4 are consecutively encountered is specified as the top or upper surface, and the opposite surface is subsequently referred to as the bottom or lower surface. A set of topolographical markers is introduced to either surface of the rectangular origami tile at six unique positions, labeled as A–F in Figure 2. Each set contains six individual DNA loops with the same 28-nucleotide-long sequence, directly attached to the underlying staple strands at designated positions. The sequence is designed to fold into two stem-loop structures, forming a dumbbell shaped index. Within each group, the 6 loops are extending away from the surface of the tile in the same direction, upward or downward. We explore how the global curvature of the tile and, thus, superstructure formation is influenced by the presence, absence, and arrangement of loop structures. The degree of influence was evaluated from atomic force microscopy (AFM) images of superstructures formed from the various monomer units.

In the first set of experiments, the upper surfaces of the origami tiles were decorated with anywhere from one to six sets of dumbbell structures. When only group A dumbbell loops (corner 2) are introduced, the resulting superstructures exhibit no obvious differences from the unmodified origami tile system (no dumbbell structures in the monomers): straight ribbons are observed for the 1–3 connection, and twisted structures are observed for the 2–4 connection (Figure 2b), suggesting that the origami tiles do not have significantly different conformations. Similarly, when both group A and B (corner 1) loops are both displayed, straight and twisted ribbons were observed in the 1–3 and 2–4 direction, respectively. However, the degree of twisting was reduced from a half twist per 2–3 tiles to a half twist per 4–5 tiles (Figure 2c). This result is consistent with the hypothesis that the repulsive interactions among neighboring loops and, between the loops and the tile, actually reduce the out-of-plane twisting of the origami tile in the 2–4 diagonal direction.

The addition of group C loops (in the middle of the right side) results in a dramatically different 1–3 connected superstructure compared to that assembled with unmodified origami tiles; twisted superstructures are observed rather than linear ribbons. On the other hand, the 2–4 connected ribbons become further unwound (Figure 2d). This indicates that the presence of three sets of dumbbell structures extended from the upper surface induces a twisting in 1–3 connected superstructures while reducing the degree of twisting in 2–4 connected structures.

On the opposite side of the tile (the left side), the addition of group D dumbbell loops reverses the twisting in 2–4 connected superstructures, resulting in linear ribbons. Meanwhile, 1–3 connected structures appear more tightly twisted (Figure 2e). Upon further addition of group E and group F dumbbell loops, similar products were observed; however, the 1–3 connected twisted ribbon structures were shorter, likely because overtwisting in the 1–3 direction interferes with the association between the tiles. The average length and period between full twists of each structure are summarized in Table S1, Supporting Information.

On the basis of these observations, it was expected that adding dumbbell loops on the bottom surface of the origami tiles, rather than the top surface as shown above, should change the curvature of origami tiles in the opposite direction. In the same manner previously described, one to six sets of dumbbell loops were displayed on the bottom surface of the tiles (Figure 3, left), at the same positions within the tiles, except extending

downward. The AFM images shown in Figure 3 (right) reveal that the addition of linker strands (either 1–3 or 2–4 linkers) results in final structures that are nearly the same as those formed from unmodified tiles, regardless of the number or position of the dumbbell loops. A summary of the average length and period between full twists of each structure is located in Table S2. This result suggests that the repulsive interactions between dumbbell loops displayed on the bottom surface of the origami tiles do not significantly influence the global twist of the tiles, which can be understood if we assume that corners 2 and 4 curl upward in unmodified tiles.

Figure 4 contains models illustrating the proposed change in the tiles as groups of dumbbell loop are added. In summary, it is clear that unmodified tiles are somewhat concave at corners 2 and 4 (viewed from the top) (Figure 4a) due to the out of plane bending of the corners, while corners 1 and 3 appear to lie in the same plane as the rest of the tile. This is consistent with the observation that introducing loops to the convex surface (bottom) does not significantly effect the overall curvature (Figure 4b–g, right columns). In contrast, increasing the number of dumbbell loops on the concave surface (top) helps to flatten the structure and eventually results in a “flip” of the curvature in the opposite direction, likely due to the repulsion between the loops (Figure 4b–g left column).

More specifically, displaying group A and B dumbbell loops on the top surface of the origami tiles provides the necessary force to untwist the structure, although the force is not strong enough to cause significant conformational changes (Figure 4b and c, left columns). The addition of group C loops in the middle of the right side continues to drive corner 2 into the plane, while simultaneously causing corner 3 to bend out of the plane (Figure 4d, left column). The additional influence from group D loops, in the middle of the left side, allows corners 2 and 4 to become coplanar. However, this situation forces corners 1 and 3 to bend downward (Figure 4e, left column). The overall conformation of the tile follows the same trend with the addition of group E and F loops, provoking corners 1 and 3 to bend even further downward (Figure 4f and g, left columns).

It should be noted that the ensuing conformations of the origami tiles are a consequence of the collective effects of all of the loops sets, including their interactions with the origami tiles as well as among themselves. Although this provides a fairly thorough qualitative assessment, it is still difficult to predict what the effect of loops located at arbitrary positions would be. We also stress that it is difficult to visualize the particular conformation of a single origami tile in solution by AFM imaging. For AFM imaging, the structures are adsorbed to a solid mica substrate, and they are inclined to maximize contact with the hydrophilic mica surface thereby distorting their native conformations. Nevertheless, analysis of the final products of origami tile assembly by AFM does provide useful information that can be used to construct probable models of the tiles. In fact, with the help of computational tools such as caDNAno[62] and CanDo,[63] the 3D structure of DNA origami tiles can be modeled. As shown in Figure 5b, CanDo indeed predicts that unmodified rectangular shaped origami tiles will adopt a structure with corners 2 and 4 bent upward out of the plane while corners 1 and 3 remain largely in the plane, consistent with the models shown in Figure 4a. However, all current software still lacks the ability to predict the conformation of structures that contain topographical features including DNA stem-loops.

RATIONAL DESIGN OF PLANAR ORIGAMI TILES

All the above results demonstrate that the rectangular origami tile is not perfect planar but possesses a global curvature, and this twisting can be varied by introducing other structural components, such as dumbbell loops to the structure. Therefore, we hypothesized that a planar origami tile could be achieved by deliberately selecting the number and positions of

the dumbbell loop structures within the origami tile. Considering that corners 2 and 4 are naturally bent upward, it was reasonable to predict that group A and F loops would direct the corners into the plane of the tile. However, the AFM images in Figure 6a reveal that, although tiles with group A and F loops form straight ribbons when connected by corners 1 and 3, 2–4 connected tiles form twisted ribbons. This suggests that the repulsive force provided by the two groups of loops is not sufficient to flatten the tiles. It is noted that for nontwisted stair-like ribbons, the origami tile surface can face both up and down, as evidenced in Figure 6a.

Next, in addition to groups A and F, group C and D loops were also added to the upper surface of the origami tile (Figure 6b). In this case, the 1–3 connected tiles formed twisted structures, while 2–4 connected tiles formed straight ribbons. Apparently, the repulsive force of the loops was greater than what was required to bring corners 1 and 3 into the plane, and thus, corners 1 and 3 were forced to bend downward.

The design was further modified by adding dumbbell loops to group B and E loops to the lower surface of the tile, as illustrated in Figure 6c, to compensate for the downward bending caused by the excess repulsive forces from the upper surface. AFM images reveal that both 1–3 and 2–4 connected tiles formed straight ribbons, suggesting that the overall conformation of the adapted tile is near planar. Therefore, we have demonstrated that the rational design of topographical features can be used to influence the conformation of the underlying DNA origami tile and create planar tiles. More sophisticated control over the tile structure may be possible by introducing loops to additional locations on the tile.

HETEROGENEOUS ORIGAMI FOR INFORMATION STORAGE AND COMPUTATION

As shown in Figure 3, origami tiles with various dumbbell loops decorated on the bottom surface are always assembled into straight ribbons when connected by corners 1 and 3. The reliability of this behavior can be exploited to efficiently assemble heterogeneous origami tiles, each with a unique number of dumbbell loops. When six unique origami tiles with different numbers of dumbbell loops displayed from the bottom surface were mixed in equal molar ratios and linked through corners 1 and 3, very long ribbons (up to 40 tiles long) were formed. Each of these ribbons contained a random sequence of the tiles that was easily read from the AFM images (Figure 7a). The randomness of the tile organization is a result of the equal opportunity of each tile to be incorporated at any given position.

It is possible to apply this strategy to perform parallel molecular computation by DNA tile self-assembly, in which a large number of distinct inputs may be simultaneously processed. For example, one may design individual tiles that carry sticky ends to represent two rows of input as well as one row of output, so that a truth table can be encoded. Linear self-assembly of such tiles into chains would perform XOR calculations. With a unique tile at one end of the assembly serving as the initial input, many different origami tiles can be connected by corners 1 and 3 to form straight 1D ribbons. Readout of the calculations can be achieved by AFM imaging to reveal all possible outputs.

SUMMARY AND DISCUSSION

In this study, we unambiguously revealed that the rectangular shaped origami tile based on original design parameters adopts a conformation in which the upper right (corner 2) and bottom left (corner 4) corners bend upward out of plane, which causes 2–4 connected superstructures to adopt twisted ribbon arrangements. The same nonplanar origami structure was also predicted using the software CanDo, consistent with our experimental observations.

A series of dumbbell-shaped DNA loops were introduced to the rectangular origami tiles, yielding a series of tiles with varying degrees of planarity that self-assemble into either straight or twisted ribbons. The curvature of each origami tile can be customized by deliberately displaying various structural components, such as DNA dumbbell loops, at desired locations to provide repulsive forces that will either diminish or enhance the curvature. A nearly planar rectangular origami tile was achieved through rational design, with the placement of specific numbers of dumbbell loops at certain positions on both surfaces of the tile. The linear nanoribbons may be used for many functional applications, including molecular computation or as tracks for DNA robots or circuits. Other nanoscale structural features, such as ligand protected metallic nanoparticles or inorganic nanocrystals are also known to experience repulsive interactions when they are brought into close vicinity on a DNA scaffold, and may also be used to manipulate the underlying tile.[36,64] In addition, interactions between the DNA scaffold and the selected structural components (i.e., loops, nanoparticles, etc), and among the components themselves, should be considered in the design so that precise control of the positioning, including the relative orientations, distances, and 3D geometry can be achieved.

METHODS

Materials

DNA strands were purchased from Integrated DNA Technology (www.idtdna.com) in 96-well plates, normalized to 100 μM. M13 viral DNA was purchased from New England Biolabs, Inc. (NEB, Catalog number: #N4040S). Microcon Centrifugal Filter Devices (100 000 MWCO, Catalog number: 42413) were purchased from Millipore.

Assembly of DNA Origami

The sequences used to form the unmodified rectangular DNA origami were reported previously.[39] DNA origami cores were assembled by mixing a 1:10 molar ratio of M13 viral DNA to each helper strand in 1xTAE/Mg buffer (20 mM Tris, pH 7.6, 2mM EDTA, 12.5 mM $MgCl_2$). Helper strands corresponding to the far left and right edges in each tile were not included. The final concentration of origami was 5 nM. The DNA mixtures were heated to 90 °C and slowly cooled to 4 °C in a thermal cycler over 12 h. After the formation of the origami cores, purification was performed using Microcon centrifugal filter devices (100 000 MWCO, 300*g* speed, 10 min) to remove excess helper strands. Then linker strands were added to the solution of origami cores with a 5:1 molar ratio of linker strands to core structure. The mixture was incubated at room temperature overnight.

AFM Imaging

For AFM imaging, 2 μL of sample was deposited onto a freshly cleaved piece of mica (Ted Pella, Inc.) and left for 2 min. Thirty microliters of 1xTAE/Mg buffer was then deposited onto the mica surface. Imaging was performed using a MultiMode V AFM (Veeco Instruments, now Bruker) in tapping mode, with SNL tips (Veeco Probes).

Supplementary Material

Refer to Web version on PubMed Central for supplementary material.

Acknowledgments

This work was partly supported by grants from the NSF, ONR, and ARO to Y.L. and H.Y. Y.L. and H.Y. were also supported by the Center for Bio-Inspired Solar Fuel Production, an Energy Frontier Research Center funded by the U.S. Department of Energy, Office of Science, Office of Basic Energy Sciences under Award Number DE-SC0001016. This work was also supported by State Scholarship Fund from China Scholarship Council to L.W.

H.Y. also acknowledges a grant from the NSFC (21028005) and a Wong Kwan Cheng education foundation scholarship.

References

1. Seeman NC. Nature. 2003; 421:427–431. [PubMed: 12540916]
2. Gothelf KV, LaBean TH. Org Biomol Chem. 2005; 3:4023–4037. [PubMed: 16267576]
3. Aldaye FA, Palmer A, Sleiman HF. Science. 2008; 321:1795–1799. [PubMed: 18818351]
4. Lin C, Liu Y, Yan H. Biochemistry. 2009; 48:1663–1674. [PubMed: 19199428]
5. Fu TJ, Seeman NC. Biochemistry. 1993; 32:3211–3220. [PubMed: 8461289]
6. Winfree E, Liu F, Wenzler LA, Seeman NC. Nature. 1998; 394:539–544. [PubMed: 9707114]
7. Mao C, Sun W, Seeman NC. J Am Chem Soc. 1999; 121:5437–5443.
8. LaBean TH, Yan H, Kopatsch J, Liu F, Winfree E, Reif JH, Seeman NC. J Am Chem Soc. 2000; 122:1848–1860.
9. Yan H, Park SH, Finkelstein G, Reif JH, LaBean TH. Science. 2003; 301:1882–1884. [PubMed: 14512621]
10. Liu D, Wang M, Deng Z, Walulu R, Mao C. Tensegrity J Am Chem Soc. 2004; 126:2324–2325.
11. Ding B, Sha R, Seeman NC. J Am Chem Soc. 2004; 126:10230–10231. [PubMed: 15315420]
12. Rothemund PWK, Papadakis N, Winfree E. PLoS Biol. 2004; 2:2041–2053.
13. Chelyapov N, Brun Y, Gopalkrishnan M, Reishus D, Shaw B, Adleman L. J Am Chem Soc. 2004; 126:13924–13925. [PubMed: 15506744]
14. Rothemund P, Ekani-Nkodo A, Papadakis N, Kumar A, Fygenson D, Winfree E. J Am Chem Soc. 2004; 126:16344–16352. [PubMed: 15600335]
15. Mitchell JC, Harris JR, Malo J, Bath J, Turberfield AJ. J Am Chem Soc. 2004; 126:16342–14363. [PubMed: 15600334]
16. Malo J, Mitchell JC, Venien-Bryan C, Harris JR, Wille H, Sherratt DJ, Turberfield AJ. Angew Chem, Int Ed. 2005; 44:3057–3061.
17. Mathieu F, Liao S, Kopatsch J, Wang T, Mao C, Seeman NC. Nano Lett. 2005; 5:661–665. [PubMed: 15826105]
18. Park SH, Barish R, Li H, Reif JH, Finkelstein G, Yan H, LaBean TH. Nano Lett. 2005; 5:693–696. [PubMed: 15826110]
19. Ke Y, Liu Y, Zhang J, Yan H. J Am Chem Soc. 2006; 128:4414–4421. [PubMed: 16569019]
20. Chen J, Seeman NC. Nature. 1991; 350:631–633. [PubMed: 2017259]
21. Zhang Y, Seeman NC. J Am Chem Soc. 1994; 116:1661–1669.
22. Goodman RP, Berry RM, Turberfield AJ. Chem Commun. 2004:1372–1373.
23. Shih WM, Quispe JD, Joyce GF. Nature. 2004; 427:618–621. [PubMed: 14961116]
24. Goodman RP, Schaap IAT, Tardin CF, Erben CM, Berry RM, Schmidt CF, Turberfield AJ. Science. 2005; 310:1661–1665. [PubMed: 16339440]
25. He Y, Ye T, Su M, Zhang C, Ribbe AE, Jiang W, Mao C. Nature. 2008; 452:198–201. [PubMed: 18337818]
26. Zheng J, Birktoft JJ, Chen Y, Wang T, Sha R, Constantinou PE, Ginell SL, Mao C, Seeman NC. Nature. 2009; 461:74–77. [PubMed: 19727196]
27. Mirkin CA, Letsinger RL, Mucic RC, Storhoff JJ. Nature. 1996; 382:607–609. [PubMed: 8757129]
28. Alivisatos AP, Johnsson KP, Peng X, Wilson TE, Loweth CJ, Bruchez MP Jr, Schultz PG. Nature. 1996; 382:609–611. [PubMed: 8757130]
29. Le JD, Pinto Y, Seeman NC, Musier-Forsyth K, Taton TA, Kiehl RA. Nano Lett. 2004; 4:2343–2347.
30. Li H, Park SH, Reif JH, LaBean TH, Yan H. J Am Chem Soc. 2004; 126:418–419. [PubMed: 14719910]
31. Sharma J, Chhabra R, Liu Y, Ke Y, Yan H. Angew Chem, Int Ed. 2006; 45:730–735.
32. Zheng J, Constantinou PE, Micheel C, Alivisatos AP, Kiehl PA, Seeman NC. Nano Lett. 2006; 6:1502–1504. [PubMed: 16834438]

33. Chhabra R, Sharma J, Ke Y, Liu Y, Rinker S, Lindsay S, Yan H. J Am Chem Soc. 2007; 129:10304–10305. [PubMed: 17676841]
34. Sharma J, Chhabra R, Andersen CS, Gothelf KV, Yan H, Liu Y. J Am Chem Soc. 2008; 130:7820–7821. [PubMed: 18510317]
35. Rinker S, Ke Y, Liu Y, Chhabra R, Yan H. Nat Nanotechnol. 2008; 3:418–422. [PubMed: 18654566]
36. Sharma J, Chhabra R, Cheng A, Brownell J, Liu Y, Yan H. Science. 2009; 323:112–116. [PubMed: 19119229]
37. Bhatia D, Mehtab S, Krishnan R, Indi SS, Basu A, Krishnan Y. Angew Chem, Int Ed. 2009; 48:4134–4137.
38. Mastroianni AJ, Claridge SA, Alivisatos PA. J Am Chem Soc. 2009; 131(24):8455–8459. [PubMed: 19331419]
39. Rothemund PWK. Nature. 2006; 440:297–302. [PubMed: 16541064]
40. Anderson ES, Dong M, Nielsen MM, Jahn K, Subramani R, Mamdouh W, Golas Mm, Sander B, Stark H, Oliveira CLP, et al. Nature. 2009; 459:73–76. [PubMed: 19424153]
41. Douglas SM, Dietz H, Liedl T, Högberg B, Graf F, Shis WM. Nature. 2009; 459:414–418. [PubMed: 19458720]
42. Dietz H, Douglas SM, Shih WM. Science. 2009; 325:725–730. [PubMed: 19661424]
43. Pound E, Ashton JR, Becerril HA, Woolley AT. Nano Lett. 2009; 9:4302–4305. [PubMed: 19995086]
44. Kuzuya A, Komiyama M. Chem Commum. 2009; 28:4182–4184.
45. Ke Y, Douglas SM, Liu M, Sharma J, Cheng A, Leung A, Liu Y, Shih WM, Yan H. J Am Chem Soc. 2009; 131:15903–15908. [PubMed: 19807088]
46. Zhao Z, Yan H, Liu Y. Angew Chem, Int Ed. 2010; 49:1414–1417.
47. Liedl T, Högberg B, Tytell J, Ingber DE, Shih WM. Nat Nanotechnol. 2010; 5:520–524. [PubMed: 20562873]
48. Han D, Pal S, Liu Y, Yan H. Nat Nanotechnol. 2010; 5:712–717. [PubMed: 20890274]
49. Ke Y, Lindsay S, Chang Y, Liu Y, Yan H. Science. 2008; 319:180–183. [PubMed: 18187649]
50. Shen W, Zhong H, Neff D, Norton ML. J Am Chem Soc. 2009; 131:6660–6661. [PubMed: 19400586]
51. Kuzyk A, Laitinen KT, Törmä P. Nanotechnology. 2009; 2:235305–235310. [PubMed: 19448288]
52. Kuzuya A, Kimura M, Numajiri K, Koshi N, Ohnishi T, Okada F, Komiyama M. ChemBioChem. 2009; 10:1811–1815. [PubMed: 19562789]
53. Maune HT, Han S, Barish RD, Bockrath M, Goddard WA III, Rothemund PWK, Winfree E. Nat Nanotechnol. 2010; 5:61–66. [PubMed: 19898497]
54. Ding B, Deng Z, Yan H, Cabrini S, Zuckermann RN, Bokor J. J Am Chem Soc. 2010; 132:3248–3249. [PubMed: 20163139]
55. Pal S, Deng Z, Ding B, Yan H, Liu Y. Angew Chem, Int Ed. 2010; 49:2700–2704.
56. Voigt NV, Tørring T, Rotaru A, Jacobsen MF, Ravnsbæk JB, Subramani R, Mamdouh W, Kjems J, Mokhir A, Basenbacher F, et al. Nat Nanotechnol. 2010; 5:200–203. [PubMed: 20190747]
57. Lund K, Manzo AJ, Dabby N, Michelotti N, Johnson-Buck A, Nangreave J, Taylor S, Pei R, Stojanovic MN, Walter NG, Winfree E, Yan H. Nature. 2010; 465:206–210. [PubMed: 20463735]
58. Endo M, Sugita T, Katsuda Y, Hidaka K, Sugiyama H. Chem—Eur J. 2010; 16:5362–5368. [PubMed: 20391568]
59. Liu W, Zhong H, Wang R, Seeman NC. Angew Chem, Int Ed. 2011; 50:264–267.
60. Li Z, Liu M, Wang L, Nangreave J, Yan H, Liu Y. J Am Chem Soc. 2010; 132:13545–13552. [PubMed: 20825190]
61. Jungmann R, Scheible M, Kuzyk A, Pardatscher G, Castro CE, Simmel FC. Nanotechnology. 2011; 22:275301. [PubMed: 21597145]
62. Douglas SM, Marblestone AH, Teerapittayanon S, Vazquez A, Church GM, Shih WM. Nucleic Acids Res. 2009; 37:5001–5006. [PubMed: 19531737]

63. Castro CE, Kilchherr F, Kim D, Shiao EL, Wauer T, Wortmann P, Bathe M, Dietz H. Nat Methods. 2011; 8:221–229. [PubMed: 21358626]

64. Zhang J, Liu Y, Ke Y, Yan H. Nano Lett. 2006; 6:248–251. [PubMed: 16464044]

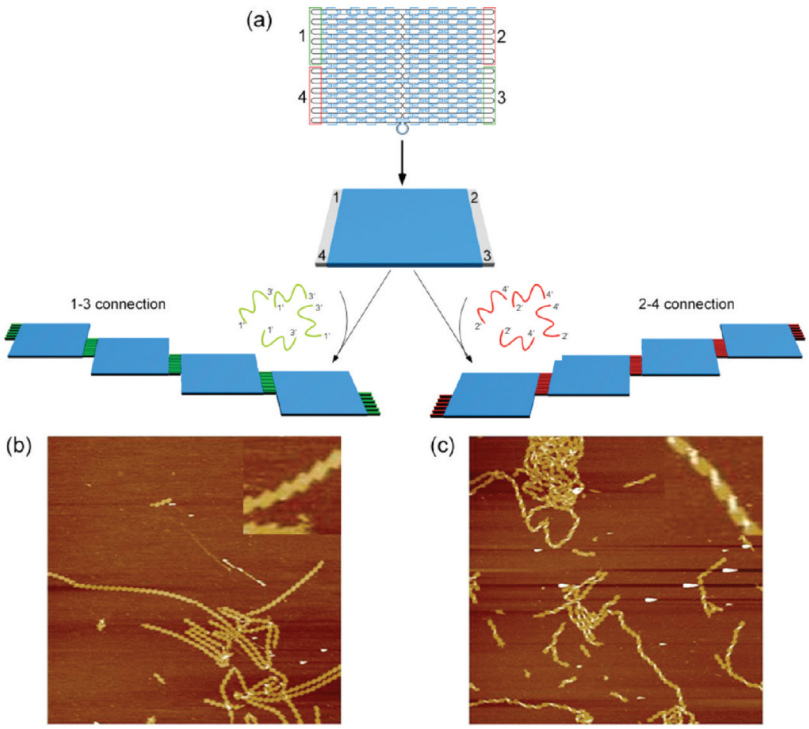

Figure 1.

1D stair-like DNA ribbons assembled from rectangular origami tiles. (a) The origami tile cores are assembled with the staple strands on the left and right edges omitted. The four corners that contain sections of unpaired M13 are denoted 1, 2, 3, and 4, each spanning 12 helices. Two sets of linker strands are designed to join corners 1 and 3, or 2 and 4, respectively. After the addition of a set of 12 1′–3′ linkers to preassembled origami cores, the tiles are diagonally connected to form stair-like ribbons in the 1–3 direction. Similarly, a set of 2′–4′ linkers connect origami cores in the 2–4 direction (where 1′ denotes complementarity with corner 1). (b) AFM images of long DNA ribbons formed from rectangular origami connected by corners 1 and 3. (c) AFM images of right-handed spiral ribbons formed by origami tiles connected by corners 2 and 4. All AFM images are 5 μm×5 μm. Insets in are zoom-in images, 300 nm ×300 nm.

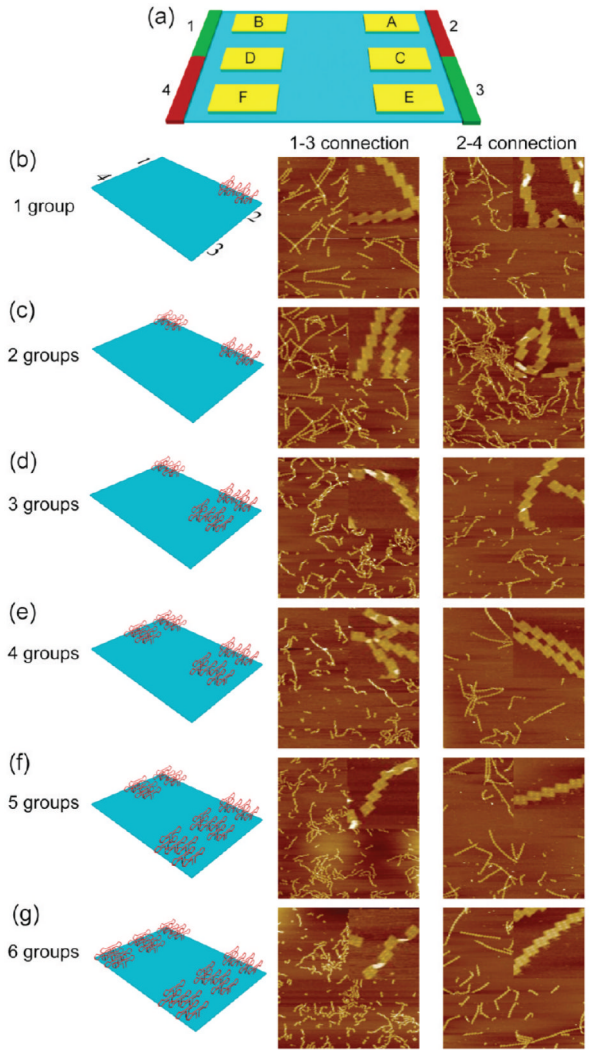

Figure 2.

AFM images of 1D DNA ribbons assembled from rectangular origami tiles with different numbers of dumbbell loops on the top surface. (a) Scheme shows the position of each of the 6 sets of loops (in yellow) on the origami tile (in blue). (b) The display of group A loops on origami tiles does not substantially change their association. Straight ribbons are formed from 1–3 connected tiles, while 2–4 connected tiles form twisted structures. (c) After the addition of group B loops, sections of the 2–4 connected ribbons are unwound. (d) The addition of group C loops results in twisted ribbons in 1–3 connected tiles, and additional sections of 2–4 connected ribbons are unwound. (e) With addition of group D loops, straight ribbons are assembled from 2–4 connected tiles, and twisted ribbons are observed from 1–3 connected tiles. (f,g) The addition of group E and F loops results in a shortening of 1–3 connected ribbons. All AFM images are 5 μm×5 μm. Insets in are zoom-in images, 500 nm×500 nm; each bright spot on origami tiles represents one group of dumbbell loops that contains six individual loops.

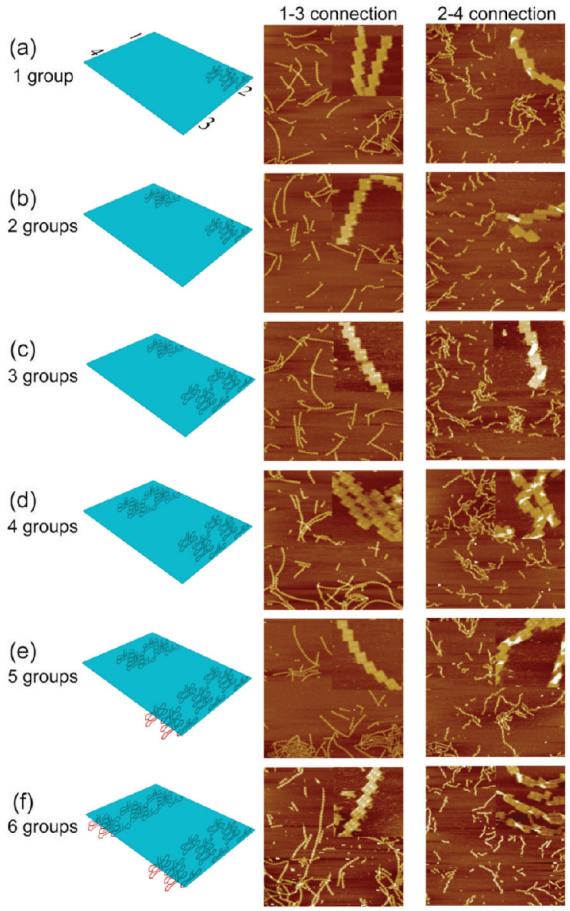

Figure 3.
AFM images of 1D DNA ribbons assembled from the rectangular origami tiles with different numbers of dumbbell loops on the bottom surface. (a–f) The addition of loops has no effect on the final structures that are assembled in either direction. In all cases, straight ribbons are formed from 1–3 connected tiles, while twisted structures are assembled from 2–4 connected tiles, the same as for the unmodified tiles. All AFM images are 5 μm × 5 μm. Insets in are zoom-in images, 500 nm×500 nm; each bright spot on origami tiles represents one group of dumbbell loops.

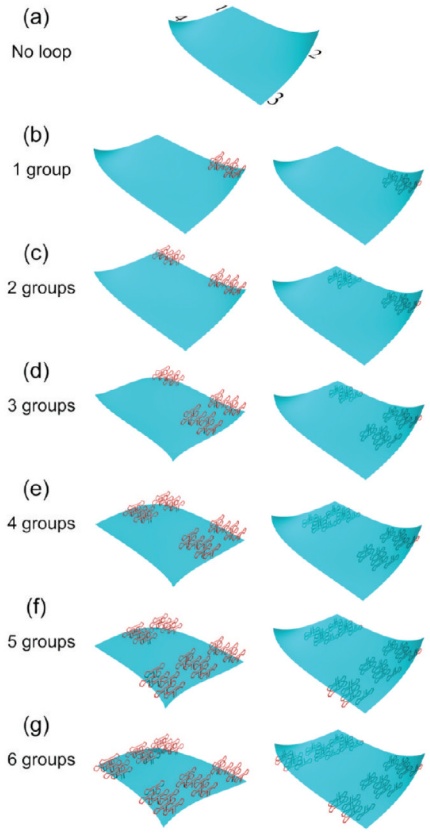

Figure 4.

Control of the conformation of a DNA origami tile through the addition of topographical features. (a) The unmodified origami tile has a twisted conformation in which corners 2 and 4 bend upward. (b,c) The addition of group A and B loops result in no significant conformational changes, regardless of which surface they are displayed on. (d) When group C loops are added to the upper surface, corners 1 and 3 begin to bend downward. (e) The addition of group D loops to the upper surface results in a coplanar organization of corners 2 and 4. (f,g) The addition of group E and F loops to the upper surface causes additional downward bending of corners 1 and 3. There are no significant conformational changes when the loops are added to the lower surface.

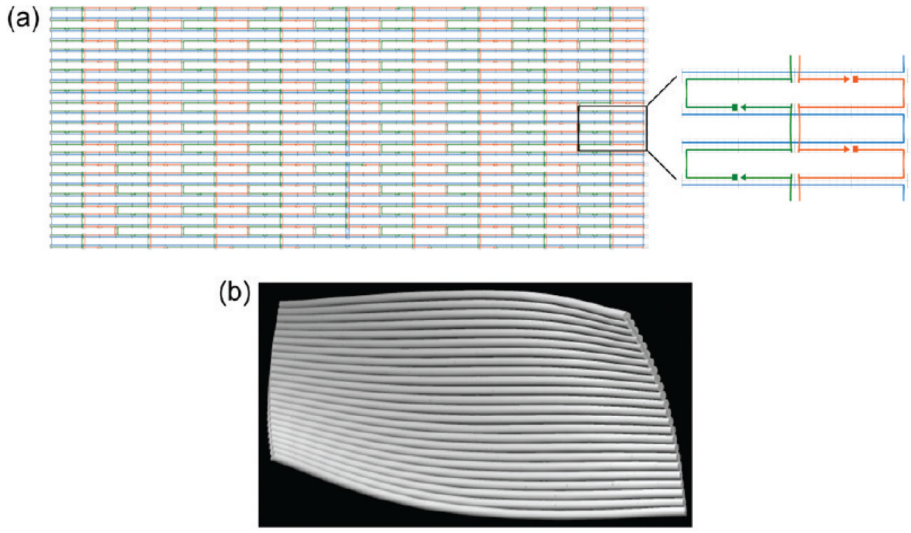

Figure 5.
Predicted structural model of the rectangular shaped DNA origami tile. (a) caDNAno design diagram of unmodified rectangular DNA origami. (b) CanDo analysis predicts that the rectangular origami tile exhibits a nonplanar conformation in which corners 2 and 4 bend upward out of the plane, while corners 1 and 3 remain in plane.

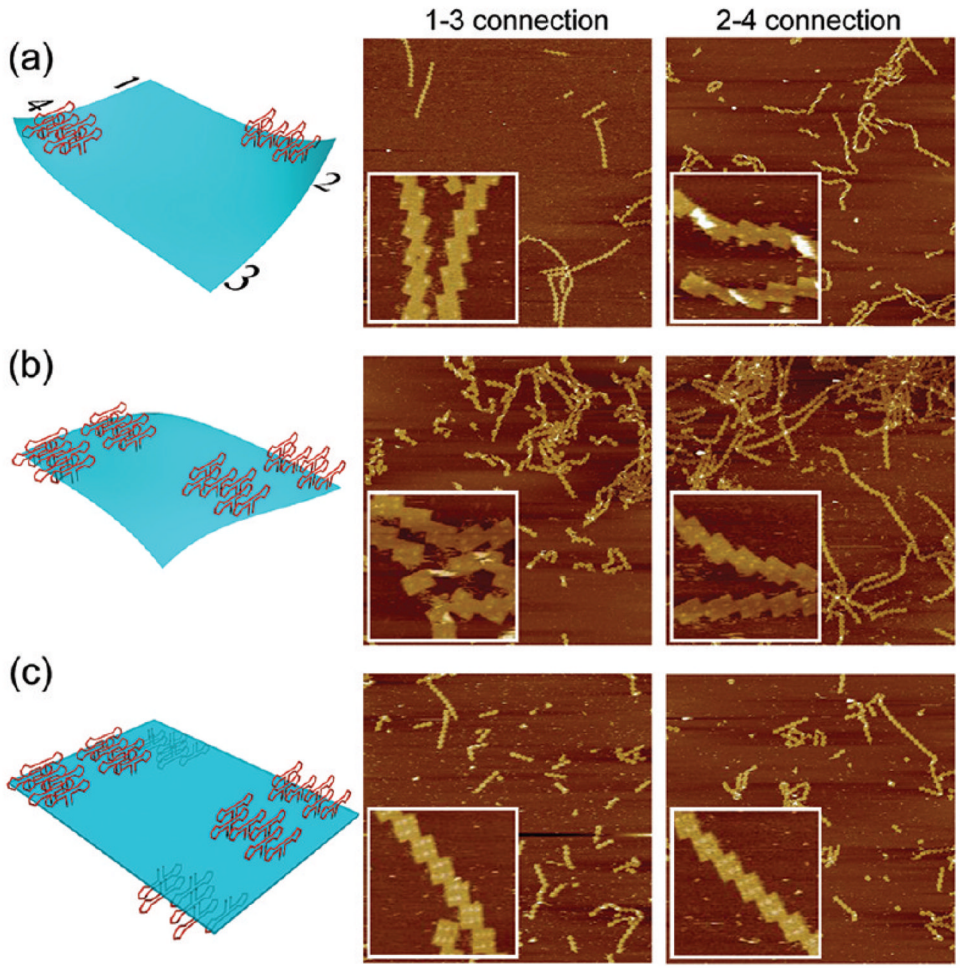

Figure 6.

A planar rectangular origami tile was achieved by controlling the number and position of dumbbell loops. (a) Adding group A and F loops to the upper surface did not disrupt the upward bending at the corners 2 and 4. (b) The addition of group C and D loops overcorrected the bending and caused corners 1 and 3 to bend downward. (c) With groups A, C, D and F loops on the upper surface and groups B and E on the lower surface, the overall tile is nearly planar. All AFM images are 5 μm × 5 μm. Insets in are zoom-in images, 500 nm × 500 nm; each bright spot on origami tiles represents one group of dumbbell loops.

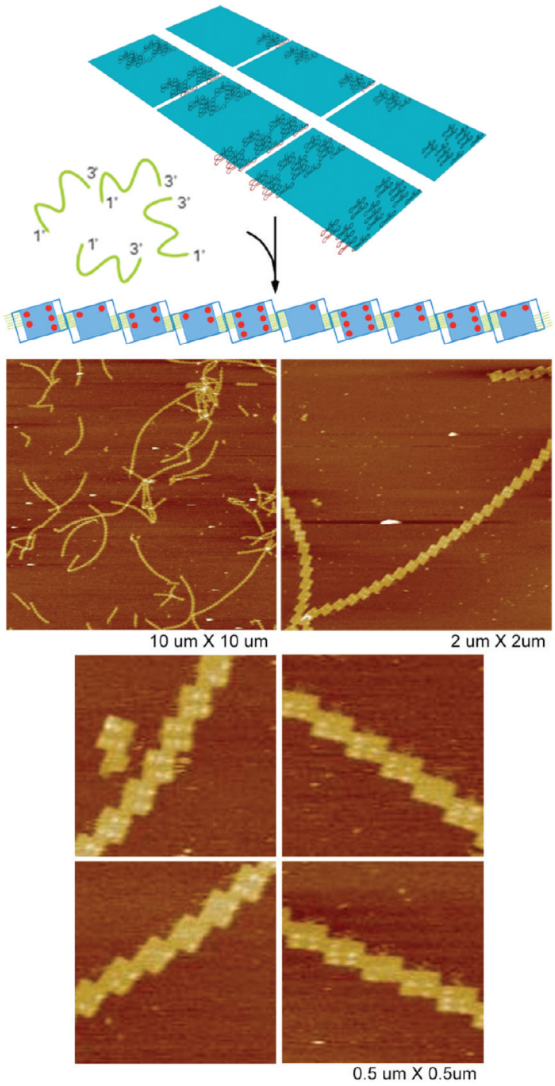

Figure 7.
Heterogeneous assembly of six different origami tiles decorated with one to six dumbbell loops on the bottom surface, connected by corners 1 and 3 to form very long ribbons. Scales of AFM images are labeled.